Experimental Evaluation of Three Fixed-Camera Visual Servo Controllers on a Robot–Pendulum

MARCO MENDOZA, FERNANDO REYES & ISELA BONILLA
Grupo de Robótica, Facultad de Ciencias de la Electrónica
Benemérita Universidad Autónoma de Puebla
Apartado Postal 542, Puebla 72001
Tel/Fax: +52 222 29 55 00 ext. 7410
MÉXICO

Abstract: - This paper addresses the visual servoing problem of a robot–pendulum in fixed–camera configuration. We present two new visual position controllers supported by a rigorous analysis of local asymptotic stability in agreement with the Lyapunov's direct method and the LaSalle's invariance principle. The proposed controllers belong to the family of Transpose Jacobian-based schemes. We also present the experimental evaluation of three visual servo controllers on a direct–drive robot–pendulum.

Key-Words: - Visual servoing, Fixed–Camera, Visual controllers, Lyapunov function.

1 Introduction

Visual Information is a useful robotic sensor since it mimics the human sense of vision and allows for noncontact measurement of the environment. Machine vision can provide closed–loop position control for a robot end-effector, this is referred to as *visual servoing*. This term was first introduced by Hill and Park [1] in 1979 to distinguish their experiments when the system alternated between picture taking and moving [2].

Visual servoing is the use of the visual information in the feedback loop to control the end-effector either relative to a target object. Visual servoing represents an attractive solution to position control of robots manipulators [3] [4].

This paper addresses the visual positioning problem when the object is static. We present for the fixed-camera configuration two new vision controllers to deliver bounded control actions belonging to the Transpose Jacobian-based family, philosophy first introduced by Takegaki and Arimoto [5] to solve the regulation problem in Cartesian space. The new control schemes are supported by a rigorous proof, this is, it is proved that visual positioning control errors converge asymptotically to zero in local sense.

Although the main contribution of the work are the proposed controllers with their corresponding stability proof, the paper also includes the experimental evaluation of three visual servo controllers belonging to the Transpose Jacobian–based family on a direct–drive robot–pendulum.

This paper is organized as follows. Section 2 presents the robot dynamics. In Section 3 is included the problem formulation and its stability proof. Section 4 describes the experimental set-up. The experimental results are presented in Section 5. Finally, we offer some conclusions in Section 6.

2 Robotic system model

The robotic system considered in this paper is composed by a direct–drive robot–pendulum and a vision system including a fixed camera as depicted in Figure 1.

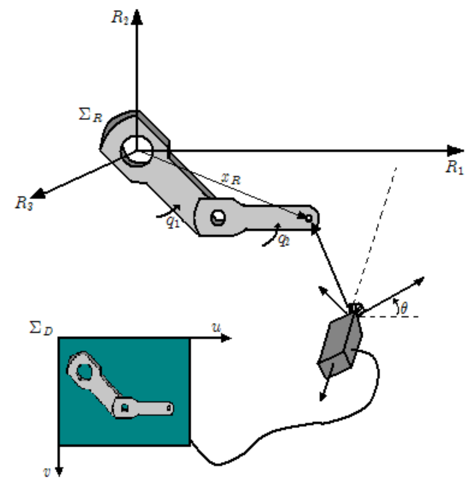

Figure 1: Robotic system

2.1 Robot kinematics

Kinematics describe the analytic relation between the joint positions and the robot end-effector posture [6].

Direct kinematics is a vectorial function that relate joint coordinates with Cartesian coordinates

$$\boldsymbol{f} : \mathbb{R}^n \rightarrow \mathbb{R}^m$$

where n is the number of degrees of freedom, and m represents the dimension of the Cartesian coordinate frame.

The direct kinematics gives the position $\boldsymbol{x}_R \in \mathbb{R}^2$ of end-effector with respect to the robot coordinate frame ($x_{R3} = 0$)in terms of the joint positions:

$$\boldsymbol{x}_R \quad = \quad f(\boldsymbol{q}). \tag{1}$$

The so-called analytical Jacobian matrix $J(\boldsymbol{q}) \in \mathbb{R}^{n \times 2}$ of the robot is defined from direct kinematics as

$$J_A(\boldsymbol{q}) \quad = \quad \frac{\partial f(\boldsymbol{q})}{\partial \boldsymbol{q}}. \tag{2}$$

2.2 Robot dynamics

Derivation of the dynamic model of a robot manipulator plays an important role for simulation of motion, analysis of manipulator structures, and design of control algorithms. Dynamic equation of a n degrees of freedom robot in absence of friction or other disturbances, in agreement with the Euler-Lagrange methodology [7], is given for

$$M(\boldsymbol{q})\ddot{\boldsymbol{q}} + C(\boldsymbol{q}, \dot{\boldsymbol{q}})\dot{\boldsymbol{q}} + \boldsymbol{g}(\boldsymbol{q}) = \boldsymbol{\tau} \tag{3}$$

where $\boldsymbol{q}$ is the $n \times 1$ vector of joint displacements, $\dot{\boldsymbol{q}}$ is the $n \times 1$ vector of joint velocities, $\boldsymbol{\tau}$ is the $n \times 1$ vector of applied torques, $M(\boldsymbol{q})$ is the $n \times n$ symmetric positive definite manipulator inertia matrix, $C(\boldsymbol{q}, \dot{\boldsymbol{q}})$ is the $n \times n$ matrix of centripetal and Coriolis torques, and $\boldsymbol{g}(\boldsymbol{q})$ is the $n \times 1$ vector of gravitational torques.

The equation of dynamic model (3) is very complex, however exists fundamental properties [8] that can used to design new control algorithms.

2.3 Vision system model

The goal of a machine vision system is to create a model of the real world from images. A machine vision system recovers useful information about a scene from its two-dimensional projections. Since images are two-dimensional projections of the three-dimensional world. This recovery requires the inversion of a many-to-one mapping [9].

Vision system model relate the coordinates of the Σ_R robot manipulator frame with the coordinates of the Σ_D computer screen frame in pixels. This model define a set of right-hand Cartesian frames.

Let $\Sigma_R = \{R_1, R_2, R_3\}$ be a Cartesian frame attached to the robot base. Where the axes R_1 and R_2 represent the robot workspace.

A TV camera (CCD type) has a $\Sigma_C = \{C_1, C_2, C_3\}$ Cartesian frame, whose origin is attached at the intersection of the optical axis with respect the geometric center of Σ_C. The description of a point in the camera frame is denoted by x_C. The position of the camera frame with respect to Σ_R is denoted by $o_C = [o_{C_1}, o_{C_2}, o_{C_3}]^T$. It is assumed that the camera frame possesses a rotation θ around axis R_3.

The acquired scene is projected on the CCD, which has a reference frame denoted by $\Sigma_I = \{I_1, I_2\}$, whose origin is attached at the geometric center of the CCD. The axes I_1 and I_2 are parallel with respect to the axes C_1 and C_2 respectively.

To obtain the coordinates of the image at the plane CCD a perspective transformation is required.

Finally the image of the scene on the CCD is digitalized and transferred to the computer memory and displayed on the computer screen. We define a new two dimensional computer image coordinated frame $\Sigma_D = \{\text{u, v}\}$, whose origin is attached at the upper left corner of the computer screen. Therefore the *fixed-camera* vision system model is given by:

$$\begin{aligned}\begin{bmatrix} u \\ v \end{bmatrix} &= \begin{bmatrix} -\alpha_u & 0 \\ 0 & \alpha_v \end{bmatrix} \Bigg(\frac{\lambda}{\lambda - o_{C_3}} R(\theta)^T \\ &\quad \left[\begin{bmatrix} x_{R_1}(\boldsymbol{q}) \\ x_{R_2}(\boldsymbol{q}) \end{bmatrix} - \begin{bmatrix} o_{C_1} \\ o_{C_2} \end{bmatrix} \right] \Bigg) \qquad (4) \\ R(\theta) &= \begin{bmatrix} \cos\theta & -\sin\theta \\ \sin\theta & \cos\theta \end{bmatrix} \qquad (5)\end{aligned}$$

where $\alpha_u > 0$, $\alpha_v > 0$ are the scale factors in pixels/m, $R(\theta) \in SO(2)$ is the rotation matrix which represents the orientation of the camera with respect to the world frame Σ_R, and $\lambda > 0$ is the focal length of the camera.

The vision system model presented consider the next hypothesis:

1. The axis R_3 of the robot frame is parallel with respect to the axis C_3 of the camera frame $(C_3 \| R_3)$. Furthermore the planes $R_1 - R_2$ and $C_1 - C_2$ are also parallels $(R_1 - R_2 \| C_1 - C_2)$ and exists a rotation θ around the axis R_3 by denote the orientation between both coordinated frames.

2. The plane CCD is orthogonal to the optical axis, therefore the planes $C_1 - C_2$ and $I_1 - I_2$ are parallels $(C_1 - C_2 \| I_1 - I_2)$.

3. The camera possesses a perfect aligned optical system and free of optical aberrations, therefore the optical axis intersects at the geometric center of the plane CCD.

3 Control problem formulation

The control problem using visual information for the fixed-camera configuration can be defined as to move the robot end-effector in such a way that reaches the desired object visually captured by the camera in its working space [10].

Since that in the fixed-camera configuration the vision system includes whole panoramic scenes of robot workspace, thus is possible locate the robot end-effector as well as the target. In a image-based system the robot task is specified in the image plane in terms of image features corresponding to observable point rigidly attached to the robot end-effector. It is assumed that the target resides in the plane $R_1 - R_2$, depicted in Figure 1. Let $[u_d \; v_d]^T$ the description with respect to the computer image frame Σ_D.

The control problem in visual servoing consists in to design a control law τ in such a way that the image feature $[u \; v]^T$ corresponding to the end-effector reaches the desired image feature $[u_d \; v_d]^T$ of the target.

The image feature error is defined as

$$\begin{bmatrix} \tilde{u} \\ \tilde{v} \end{bmatrix} = \begin{bmatrix} u_d - u \\ v_d - v \end{bmatrix} \qquad (6)$$

therefore, the control aim is to assure that $\lim_{t\to\infty}$ $[\tilde{u}(t) \; \tilde{v}(t)]^T = 0 \quad \in \; \mathbb{R}^2$, at least for initial conditions $[\tilde{u}(0) \; \tilde{v}(0)]^T$ and $\dot{q}(0)$ sufficiently small [3].

The control problem is solvable if exists a joint motion $\boldsymbol{q}_d(t) \in \mathbb{R}^2$ such that

$$\begin{aligned}\begin{bmatrix} u_d \\ v_d \end{bmatrix} &= \begin{bmatrix} -\alpha_u & 0 \\ 0 & \alpha_v \end{bmatrix} \Bigg(\frac{\lambda}{\lambda - o_{C_3}} R(\theta)^T \\ &\quad \left[\begin{bmatrix} x_{R_1}(\boldsymbol{q}_d) \\ x_{R_2}(\boldsymbol{q}_d) \end{bmatrix} - \begin{bmatrix} o_{C_1} \\ o_{C_2} \end{bmatrix} \right] \Bigg) . \qquad (7)\end{aligned}$$

To solve the visual position control problem, we present the following controllers:

$$\begin{aligned}\boldsymbol{\tau}_1 &= J_A^T(\boldsymbol{q}) R(\theta) K_p \arctan\left(\Lambda \begin{bmatrix} \tilde{u} \\ \tilde{v} \end{bmatrix} \right) - K_v \arctan(\Lambda \dot{\boldsymbol{q}}) \\ &+ \boldsymbol{g}(\boldsymbol{q}), \qquad (8)\end{aligned}$$

$$\boldsymbol{\tau}_2 = \boldsymbol{f}(K_p, \tilde{u}, \tilde{v}) - K_v \dot{\boldsymbol{q}} + g(\boldsymbol{q}), \qquad (9)$$

where K_p represents the $\mathbb{R}^n \times \mathbb{R}^n$ diagonal matrix of proportional gains, K_v represents the $\mathbb{R}^n \times \mathbb{R}^n$ diagonal matrix of derivative gains, and Λ is a $\mathbb{R}^n \times$

$\mathbb{R}^n$ diagonal matrix.

$$\boldsymbol{f}(K_p,\tilde{u},\tilde{v}) = \begin{bmatrix} f_1(K_p,\tilde{u},\tilde{v}) \\ \vdots \\ f_n(K_p,\tilde{u},\tilde{v}) \end{bmatrix}$$

$$f_i(K_p,\tilde{u},\tilde{v}) = \begin{cases} f_p(\tanh)_i & \text{if } |f_p(\sinh)_i| \geq \sigma_i^+ \\ f_p(\sinh)_i & \text{if } |f_p(\sinh)_i| < \sigma_i^+ \end{cases}$$

for all $i = 1, 2, ..., n$ and

$$\begin{bmatrix} f_p(\tanh)_1 \\ \vdots \\ f_p(\tanh)_n \end{bmatrix} = J_A^T(\boldsymbol{q}) K_p R^T(\theta) \tanh\left(\Lambda \begin{bmatrix} \tilde{u} \\ \tilde{v} \end{bmatrix}\right)$$

$$\begin{bmatrix} f_p(\sinh)_1 \\ \vdots \\ f_p(\sinh)_n \end{bmatrix} = J_A^T(\boldsymbol{q}) K_p R^T(\theta) \sinh\left(\Lambda \begin{bmatrix} \tilde{u} \\ \tilde{v} \end{bmatrix}\right).$$

Their local asymptotic stability has been shown using the following Lyapunov functions

$$\begin{aligned} V_1(\dot{\boldsymbol{q}},\tilde{u},\tilde{v}) &= \frac{1}{2}\dot{\boldsymbol{q}}^T M(\boldsymbol{q})\dot{\boldsymbol{q}} + \sum_{i=1}^{n} k_{pi} \left[\begin{bmatrix} \tilde{u} \\ \tilde{v} \end{bmatrix} \arctan \begin{bmatrix} u \\ v \end{bmatrix}\right. \\ &- \left.\frac{1}{2}\ln\left(1 + \begin{bmatrix} u \\ v \end{bmatrix}^T \begin{bmatrix} u \\ v \end{bmatrix}\right)\right], \qquad (10) \end{aligned}$$

$$V_2(\dot{\boldsymbol{q}},\tilde{u},\tilde{v}) = \frac{1}{2}\dot{\boldsymbol{q}}^T M(\boldsymbol{q})\dot{\boldsymbol{q}} + \mathcal{U}_a(K_p,\tilde{u},\tilde{v}), \qquad (11)$$

in (11) we have that

$$\mathcal{U}_a(K_p,\tilde{u},\tilde{v}) = \begin{cases} \mathcal{U}_a(\tanh) & \text{if } |f_p(\sinh)_i| \geq \sigma_i^+ \\ \mathcal{U}_a(\sinh) & \text{if } |f_p(\sinh)_i| < \sigma_i^+ \end{cases}$$

$\mathcal{U}_a(\tanh) =$

$$\begin{bmatrix} \sqrt{\ln\cosh(\gamma_1\tilde{u})} \\ \sqrt{\ln\cosh(\gamma_2\tilde{v})} \end{bmatrix}^T K_p\Gamma^{-1} \begin{bmatrix} \sqrt{\ln\cosh(\gamma_1\tilde{u})} \\ \sqrt{\ln\cosh(\gamma_2\tilde{v})} \end{bmatrix}$$

$\mathcal{U}_a(\sinh) =$

$$\begin{bmatrix} \sqrt{\cosh(\gamma_1\tilde{u}) - 1} \\ \sqrt{\cosh(\gamma_2\tilde{v}) - 1} \end{bmatrix}^T K_p\Gamma^{-1} \begin{bmatrix} \sqrt{\cosh(\gamma_1\tilde{u}) - 1} \\ \sqrt{\cosh(\gamma_2\tilde{v}) - 1} \end{bmatrix}.$$

In the two Lyapunov functions $\Gamma = K\Lambda = \text{diag}\{\gamma_1, \gamma_2\}$ where $K = \text{diag}\{-\frac{\alpha_u\lambda}{\lambda - o_{C_3}}, -\frac{\alpha_v\lambda}{\lambda - o_{C_3}}\}$ and both are diagonal positive definite matrices.

The time derivates of (10) and (11) are given by

$$\dot{V}_1(\dot{\boldsymbol{q}},\tilde{u},\tilde{v}) = -\dot{\boldsymbol{q}}^T K_v \arctan(\Lambda\dot{\boldsymbol{q}}) \leq 0, \qquad (12)$$

$$\dot{V}_2(\dot{\boldsymbol{q}},\tilde{u},\tilde{v}) = -\dot{\boldsymbol{q}}^T K_v \dot{\boldsymbol{q}} \leq 0, \qquad (13)$$

respectively, which are negative semidefinite functions. Therefore, in agreement with the Lyapunov's direct method, the control laws yield stable closed loop systems.

In order to study asymptotic stability we can apply the LaSalle's theorem [11], in the region

$$\begin{aligned} \Omega &= \left\{ \begin{bmatrix} \begin{bmatrix} \tilde{u} \\ \tilde{v} \end{bmatrix} \\ \dot{\boldsymbol{q}} \end{bmatrix} : \dot{V}(\dot{\boldsymbol{q}},\tilde{u},\tilde{v}) = 0 \right\} \\ &= \left\{ \begin{bmatrix} \tilde{u} \\ \tilde{v} \end{bmatrix} \in \mathbb{R}^2, \text{ and } \dot{\boldsymbol{q}} = 0 \in \mathbb{R}^2 \right\} \end{aligned}$$

the invariant set has isolated equilibria for revolute joint planar robots, therefore we conclude the latter equilibria are asymptotically stable.

To propose of experimental evaluation, the controllers presented in this paper will be evaluated with the reported in [3]:

$$\begin{aligned} \boldsymbol{\tau}_3 &= J_A^T(\boldsymbol{q}) R(\theta) K_p \tanh\left(\Lambda \begin{bmatrix} \tilde{u} \\ \tilde{v} \end{bmatrix}\right) - K_v \tanh(\Lambda\dot{\boldsymbol{q}}) \\ &+ \boldsymbol{g}(\boldsymbol{q}). \qquad (14) \end{aligned}$$

4 Experimental set-up

An experimental system for research of robot control algorithms has been designed and built at The Universidad Autónoma de Puebla, México; it is a direct–drive robot pendulum (see Figure 2). The experimental robot consists of a link made of 6061 aluminum actuated by brushless direct drive servo actuator from Parker Compumotor to drive the joint without gear reduction. Advantages of this type of direct-drive actuator includes freedom from backslash and significantly lower joint friction compared with actuators composed by gear drives. The motor used in the robot are listed in Table 1.

Table 1: Servo actuator of the experimental pendulum.

Link	Model	Torque [Nm]	p/rev
Pendulum	DM1004C	4	1,024,000

The servo is operated in torque mode, so the motors act as a torque source and they accept an analog voltage as a reference of torque signal. Position information is obtained from incremental encoder located on the motor. The standard backwards difference algorithm applied to the joint position measurements was used to generate the velocity signals. The manipulator workspace is a circle with a radius of 0.35 m.

Besides position sensors and motor drivers, the robot also includes a motion control board manufactured by Precision MicroDynamic Inc., which is used to obtain the joint positions. The control algorithm runs on a Pentium–II (333 Mhz) host computer.

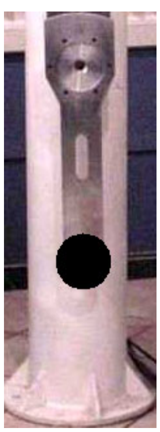

Figure 2: Experimental robot.

With reference to our direct–drive robot, only the gravitational torque is required to implement the three visual servo controllers, which is available in [12]:

$$\boldsymbol{g}(\boldsymbol{q}) \;=\; [\, 1.81\, \sin(q)\,] \quad [\mathrm{Nm}].$$

The vision system consists of a camera with a focal length $\lambda = 0.003$ [m] and a FPG-44 frame processor board that include the DSP TMS320C44. A black disc was mounted on end-effector, the centroid of disc was selected as the object feature point.

The CCD camera was placed in front of the robot arm and its position with respect to the robot frame Σ_R was $\boldsymbol{o}_C = [0.15,\ -0.25,\ 0.45]^T$ [m].

The evaluated controllers have been written in C language. The sampling rate was executed at 2.5 msec. while the visual feedback loop was at 33 msec.

5 Experimental results

We select in all controllers the desired position in the image plane as $[u_d\ v_d]^T = [533\ 296]^T$ [pixels] and the following initial position $[u(0)\ v(0)]^T = [342\ 376]^T$ [pixels] and $\dot{q}(0) = 0$ [degrees/sec]. The friction phenomena were not modeled for compensation purposes. That is, all the controllers did not show any type of friction compensation. Therefore, it was decided to consider the friction as unmodeled dynamics.

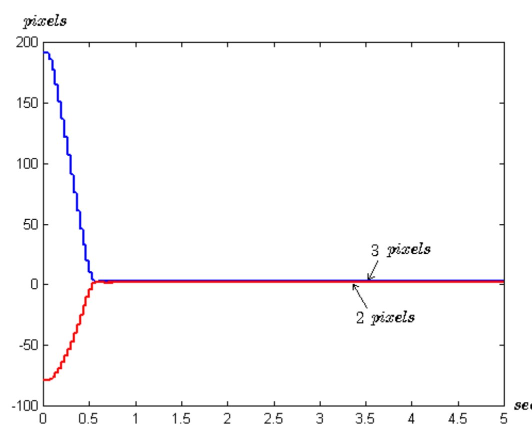

Figure 3: Feature position trajectory in the image plane for controller (8).

The experimental results for the controller (8) are shown in Figures 3-4. The proportional and derivative gains, for the controller, were selected as $K_p = 2.8$ [Nm/pixels^2], $K_v = 0.2$ [Nm-sec/degrees] respectively and $\Lambda = 0.1$. Figure 3 show that the transient response is fast and it was around 0.7 sec.

The components of the feature position error tend asymptotically to a small neighborhood of zero (3 and 2 pixels, respectively).

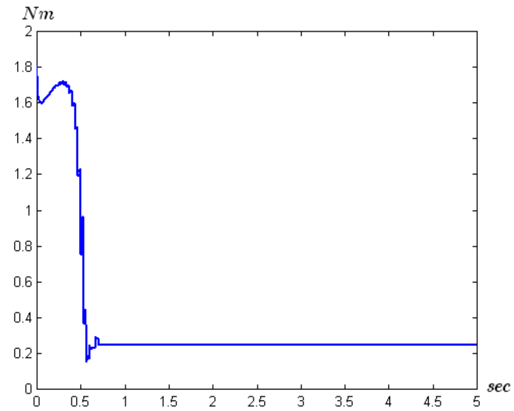

Figure 4: Applied torque for controller (8).

The applied torque for the controller (8) is shown in Figure 4. It can be observed that, in agreement with the tuning of the gains, the torque signal dont exceed the prescribed limit in Table 1.

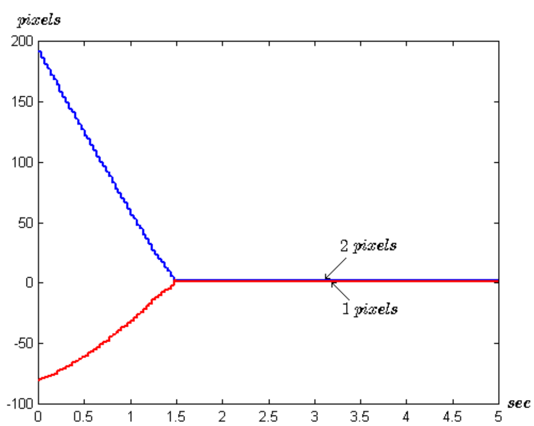

Figure 5: Feature position trajectory in the image plane for controller (9).

The experimental results for the controller (9) are shown in Figures 5-6. The gains were selected as $K_p = 4.0$ [Nm/pixels^2], $K_v = 0.029$ [Nm-sec/degrees] respectively and $\Lambda = 0.1$. The transient response was around 1.5 sec. and it is shown in the Figure 5. The components of the feature position error tend asymptotically to a small neighborhood of zero (2 and 1 pixels, respectively).

The applied torque is shown in Figure 6. It can

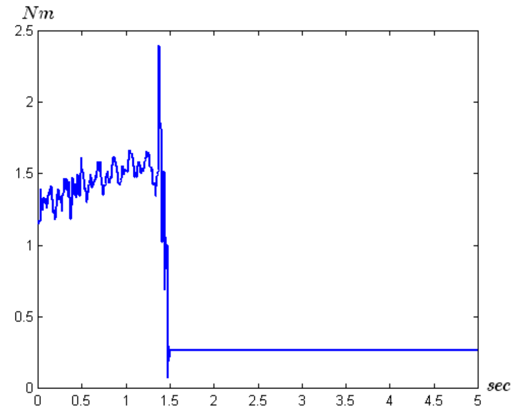

Figure 6: Applied torque for controller (9).

be observed that, in agreement with the tuning of the gains, the torque signal clearly evolve inside the prescribed limit in Table 1.

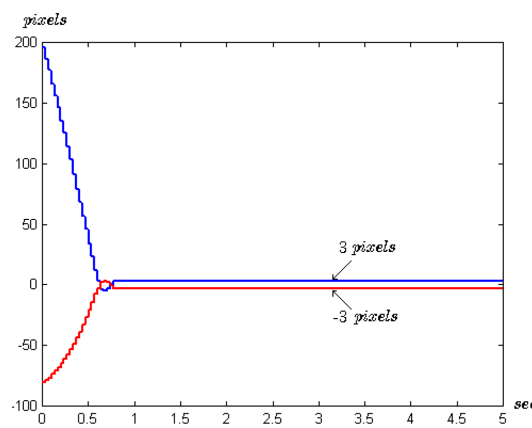

Figure 7: Feature position trajectory in the image plane for controller (14).

Finally, Figures 7-8 show the experimental results of the controller (14). The parameters of this controller were selected as $K_p = 4.0$ [Nm/pixels^2], $K_v = 0.34$ [Nm-sec/degrees] and $\Lambda = 0.1$. Figure 7 depicts the time evolution of feature error vector $[\tilde{u}\ \tilde{v}]^T$. The transient response is fast and it was around 0.8 sec. After transient, both components of the feature position error tend asymptotically to a small neighborhood (3 and -3 pixels, respectively).

The applied torque for the controller (14) is shown in Figure 8. It can be observed that, in agreement with the tuning of the gains, the torque

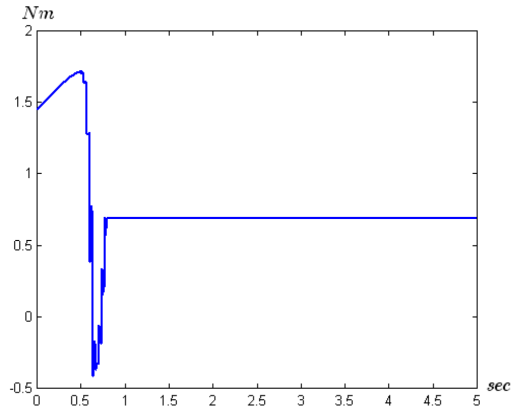

Figure 8: Applied torque for controller (14).

signal clearly evolve inside the prescribed limit in Table 1.

6 Conclusions

In this paper we have presented the analysis of local asymptotic stability and the experimental evaluation of three visual servo controllers for fixed–camera configuration. The direct visual controllers belonging to the transpose Jacobian–based family. These controllers yield locally asymptotically stable closed–loop systems.

In practical implementation of the controllers, the image processing are limited by the video rate of 33 msec. The three visual controllers show good performance in spite of the forces of friction characteristic of the mechanical system, as well as the undesirable phenomena taken place by the periods of sampling of the electronic systems employees in the system of vision.

References:

[1] Hill J. and W. T. Park, *Real Time Control of a Robot with a Mobile Camera.* in Proc. 9th ISIR, Washington, D.C., Mar. 1979, pp. 233-246.

[2] Hutchinson S., G. D. Hager and P. I. Corke, *A Tutorial on Visual Servo Control.* IEEE Trans. on Robotics and Automation, Vol. 3, No. 9, 1987, pp. 404-417.

[3] Reyes F. and R. Kelly, *Experimental Evaluation of Fixed-Camera Direct Visual Controllers on a Direct-Drive Robot.* IEEE International Conference on Robotics & Automation. Leuven, Belgium, May 1998, pp. 2327-2332.

[4] Corke P. I., *An Experimental Facility for Robotic Visual Servoing.* IEEE Region 10 Conference, Tecon 92. Melbourne, Australia, Nov. 1992, pp. 252-256.

[5] Takegaki M. and S. Arimoto, *A New Feedback Method for Dynamic Control of Manipulators.* ASME J. Dyn. Syst. Meas. Control, Vol. 103, 1981, pp. 119-125.

[6] Sciavicco L. and B. Siciliano, *Modeling and Control of Robot Manipulators.* McGraw-Hill, 1996.

[7] Spong M. W. and M. Vidyasagar, *Robots Dynamics and Control.* John Wiley & Sons, 1989.

[8] Kelly R. y V. Santibañez, *Control de Movimiento de Robots Manipuladores.* Prentice Hall, 2003.

[9] Jain R., R. Kasturi and B. G. Schunck, *Machine Vision.* McGraw Hill, 1995.

[10] Kelly R., P. Shirkey and M. W. Spong, *Fixed-Camera Visual Servo Control for Planar Robots.* IEEE International Conference on Robotics and Automation. Minneapolis, Minnesota, April 1996, pp. 2643-2649.

[11] Vidyasagar M., *Nonlinear Systems Analysis.* Englewood Cliffs, NJ: Prentice Hall, 1993.

[12] Reyes, F. & Kelly, R., *Experimental Evaluation of Identification Schemes on a Direct Drive Robot. Robotica*, Cambridge University Press. Vol. 15, 1997, pp. 563-571.